

**Wave generation and interaction with vortex motions:
sound and shock waves**

T Kambe

Department of Physics, University of Tokyo
Hongo, Bunkyo-ku, Tokyo 113, Japan

ABSTRACT Theory of vortex sound in the aeroacoustics can describe characteristic features of the waves radiated by localized vortex motions at low Mach numbers. Some experimental evidences and computational examples are presented from our studies to show remarkable agreement between observed and computed wave profiles emitted by two kinds of vortex motions in free space: *head-on* collision and *oblique* collision of two vortex rings. In the oblique collision of two vortex rings, reconnection of vortex-lines causes rapid change of geometrical structure of vortex-lines, resulting in excitation of a characteristic type of acoustic wave. As a last example, a supersonic interaction of a vortex ring with an impinging plane shock wave is presented. A computer simulation illustrates a strong local intensification of the wave caused by the presence of the vortex.

1. Introduction

Wave generation by the vorticity dynamics governed by the vorticity equation is now recognized to be formulated in the frame of the theory of *vortex sound*. Recent studies of the vortex sound are illustrated here by presenting two cases of the head-on collision and oblique collision of two vortex rings. In addition, strong interaction of a high-speed vortex ring with an impinging shock wave is described, in which remarkable local intensification of the wave is observed numerically. Characteristic Mach number in the former case is assumed to be much less than unity, while the one in the latter is larger than unity.

In the theory of vortex sound at low Mach number and high Reynolds number [1-8], the source flow is characterized by a localized vortex motion scaled on a length l representing the vortex size. This flow field is surrounded by *outer* wave field scaled on the length $\lambda \approx c\tau = O(l/M)$, where $\tau = l/u$, u being a typical velocity of the flow field. The sound speed and density in the undisturbed uniform medium are denoted by c and ρ_0 , respectively. Typical Mach number M satisfies the condition $M = u/c \ll 1$. This enables separate analysis of the two fields: *inner* flow and *outer* wave regions, because of the *compactness* of the source flow, $l \ll \lambda$.

In our investigation of the vortex sound in the past decade or so, evidences showing the validity of the theory are accumulating. Regarding the vortex collisions, the first stage of the vortex interaction is almost inviscid. This is followed by the second viscous stage : cancellation of opposite signs of vorticity at the time of head-on collision [4], reconnection of vortex-lines in the oblique collision [7, 15], and so on. Acoustic waves are generated by these motions and the waves can be detected experimentally [4, 5, 7]. Main interest here is comparison of the wave profiles thus determined computationally with the corresponding profiles determined experimentally.

2. Mathematical Formulation of Vortex Sound

Basic equation of the aerodynamic sound is given by the Lighthill's equation [8]:

$$\rho_{tt} - c^2 \nabla^2 \rho = \frac{\partial^2}{\partial x_i \partial x_j} T_{ij} \quad (1)$$

where

$$T_{ij} = \rho v_i v_j + (p - c^2 \rho) \delta_{ij} - \tau_{ij} ,$$

$\mathbf{x} = (x_i)$ is the space coordinate vector, p the pressure, ρ the density, v_i the i -th component of velocity and τ_{ij} the viscous stress tensor. Summation convention is assumed on the right hand side (rhs) of (1) and henceforth.

In the inner region scaled by the length l and time τ , the ratio of the two terms on the left hand side is estimated as $|\rho_{tt}|/|c^2 \nabla^2 p| = O(l^2/c^2 \tau^2) = O(M^2)$. In the first approximation neglecting terms of $O(M^2)$ and hence the term ρ_{tt} , the equation (1) reduces to the Navier-Stokes equation for an incompressible fluid, governing solenoidal vortex motion treated as a source flow.

In the outer region, the rhs of (1) becomes vanishingly small and the pressure is governed by the wave equation : $p_{tt} - c^2 \nabla^2 p = 0$, because of the (assumed) adiabatic relation $dp = c^2 d\rho$. In the theory [7, 10], an asymptotic representation of the velocity potential of the inner flow is given first, and then a solution of the outer wave equation is determined so as to be matched to the inner solution. The wave pressure $p^{(w)}$ matching to the inner field asymptotically as $|\mathbf{x}|/\lambda \rightarrow 0$ is given by a multi-pole expansion.

We consider the waves generated by collisions of two vortex rings in an unbounded fluid. The pressure takes a simple form in the acoustic far-field ($|\mathbf{x}|/\lambda \rightarrow \infty$). The wave pressure observed at a point $\mathbf{x} = (x_1, x_2, x_3)$ in the acoustic far-field is given as

$$p^{(w)}(\mathbf{x}, t) = -\rho_0 P_0^{(1)}(t_r) \frac{1}{r} - \frac{\rho_0}{c^2} Q_{ij}^{(3)}(t_r) \frac{x_i x_j}{r^3} + \frac{\rho_0}{c^3} Q_{ijk}^{(4)}(t_r) \frac{x_i x_j x_k}{r^4} + \dots \quad (2)$$

where superscript (n) denotes the n -th time derivative, and

$$Q_i(t) = \frac{1}{8\pi} \int (\mathbf{y} \times \boldsymbol{\omega})_i d^3y , \quad (3)$$

$$Q_{ij}(t) = -\frac{1}{12\pi} \int (\mathbf{y} \times \boldsymbol{\omega})_i y_j d^3y , \quad (4)$$

$$Q_{ijk}(t) = \frac{1}{32\pi} \int (\mathbf{y} \times \boldsymbol{\omega})_i y_j y_k d^3y , \quad (5)$$

...

$\boldsymbol{\omega} = \boldsymbol{\omega}(\mathbf{y}, t)$ is the vorticity: $\boldsymbol{\omega} = \Delta \times \mathbf{v}$, and the vector $\mathbf{x} = (x_i)$ is used for the point of observation and $\mathbf{y} = (y_i)$ for the point of integration (the source point). The resultant impulse of the vortex system is defined by $4\pi Q_i$, defined by (3), which is an invariant of motion in free space. Hence the dipole term disappears because the dipole emission is related to the rate of change of the impulse.

The second quadrupole terms (Möhring's quadrupole [3]) can be shown to derive from the non-isotropic part of the Reynolds stress $\rho_0 v_i v_j$ [11]. The first isotropic (monopole) term arises when the total kinetic energy K of the system changes, where

$$P_0(t) = -\frac{5-3\gamma}{12\pi} \frac{1}{c^2} K^{(1)}(t) , \quad K(t) = \frac{1}{2} \int v^2(\mathbf{y}, t) d^3y , \quad (6)$$

K is the total kinetic energy and γ the ratio of specific heats ($\gamma = 7/5$ for the air). K vanishes identically in an inviscid fluid. Here we have written the formula up to the third order terms. An experimental observation (described in § 4) shows existence of this order.

Using the length scale l , the vorticity scale $\omega = u/l$ and the time scale $\tau = l/u$, the scaling law of the wave pressure of the quadrupole sound is deduced as follows. The tensor Q_{ij} is normalized by $l^4 u$ and hence $Q_{ij}^{(3)}$ by $l^4 u / \tau^3 = l u^4$ (the first monopole term gives the same by (6)). Thus we find the scaling law for the quadrupole sound as

$$p_Q \sim \frac{\rho_0}{c^2} l u^4 \frac{1}{r} = \frac{\rho_0 u^4}{c^2} \frac{l}{r} .$$

The sound intensity I_Q is given by $p_Q^2/\rho_0 c$. Hence we obtain the well-known intensity law [5, 8]: $I_Q \sim (\rho_0 u^8/c^5)(l/r)^2 \propto u^8$.

3. Head-on Collision of Two Vortex Rings

Axisymmetric collision of two vortex rings [4] is a particularly simple example of the vortex sound. In an inviscid fluid, the first term of the formula (2) vanishes and the second quadrupole term reduces to

$$p = -\frac{\rho_0}{12c^2} Q^{(3)}(t_r) \frac{1}{r} (1 - 3 \cos^2 \theta), \quad Q(t) = \int \omega(\sigma, z) \sigma^2 z \, d\sigma \, dz \quad (7)$$

where $t_r = t - r/c$, and the vorticity is assumed to have only the azimuthal ϕ -component $\omega(\sigma, z)$ in the cylindrical coordinate system (z, σ, ϕ) , with $z = x_3$ and $\sigma = \sqrt{x_1^2 + x_2^2}$ and $\theta = \arccos(z/r)$. In this case the temporal behavior of the pressure is described by the single scalar function of 3rd-order derivative $Q^{(3)}(t)$, and its spatial distribution is given by $P_2^0 = (3 \cos^2 \theta - 1)/2$, an axisymmetric four-lobe directivity (Figure 1).

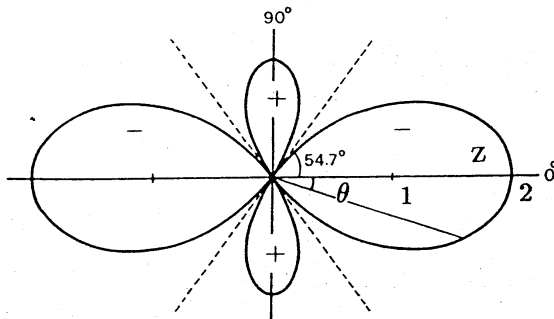


Figure 1. Directivity of the acoustic pressure: $1 - 3 \cos^2 \theta$.

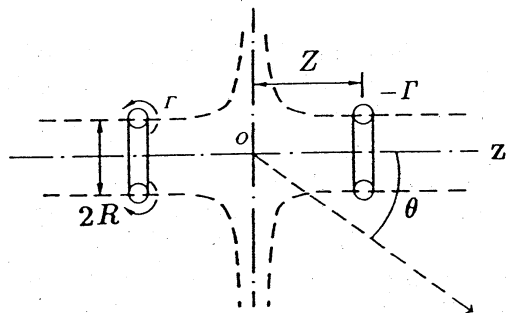


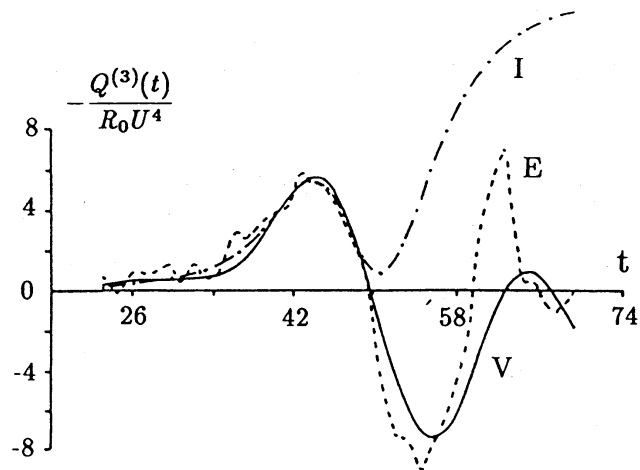
Figure 2. Head-on collision of two vortex rings (definition sketch).

Computation : Suppose that we have two vortex rings having a common symmetry axis z with one vortex being a mirror image of the other with respect to the plane $z = 0$ (Figure 2), and that they approach each other according to the equation of motion. When the vortex is characterized by its strength $-\Gamma$, ring radius $R(t)$ (core radius δ) and the distance $Z(t)$ from the symmetry plane $z = 0$, the interacting motion of two vortex rings of very thin cores is described by a system of first-order ordinary differential equations [9]. Then the profile function $Q(t)$ is expressed by $-2\Gamma R^2(t)Z(t)$. The wave pressure form is given by $Q^{(3)}(t)$, which is calculated numerically by solving the system of differential equations and shown by the curve I in Figure 3, together with the observed one E. The first peak of the profile corresponds to the initial inviscid stage of the colliding motion. Effect of finite core-size and core deformation on the wave profile is studied in detail by the inviscid contour dynamics [12]. This analysis suggests that the dip observed in the curve $-Q^{(3)}(t)$ is due to core deformation.

A numerical simulation of axi-symmetric viscous vortex collision was carried out to estimate the profile function $Q^{(3)}(t)$, shown by the curve V in Figure 3, at the Reynolds number $Re \approx 1.3 \times 10^3$, based on the initial translation velocity $U = |\dot{Z}(0)|$ and ring diameter $2R_0 = 2R(0)$ [13].

Observation : Experimental observations of the corresponding acoustic waves due to the vortex collision are reported in [4] and [14]. The Reynolds number Re was of the order 10^4 or larger in the latter study.

Figure 3.
 Temporal profiles $-Q^{(3)}(t)$;
 I : inviscid,
 E : experimental,
 V : viscous simulation.



The observed pressures at 35 stations are represented in the truncated Fourier series: $p(\theta, t) = a_0(t) + a_1(t) \cos \theta + b_1(t) \sin \theta + a_2(t) \cos 2\theta + b_2(t) \sin 2\theta$. The two terms $a_0(t)$ and $a_2(t) \cos 2\theta$ are found to be dominant and rewritten as

$$p_{mq}(\theta, t) = p_m(t) + p_q(t)(1 - 3 \cos^2 \theta),$$

where p_m and p_q represent the monopolar and quadrupolar components respectively. Significant amplitudes of $p_m(t)$ and $p_q(t)$ are detected, and $p_q(t)$ is shown as the curve E in Figure 3.

4. Oblique Collision of Two Vortex Rings

Oblique collision of two vortex rings at right angles is studied experimentally and computationally [7]. Evidently this oblique collision (Figure 4) has no axisymmetry like that in the previous case of head-on collision. At the oblique collision, opposite senses of vortex lines are forced to come into contact at the inner part. This event is followed by rapid change of vorticity structure and excitation of acoustic waves. Analysis of the wave data provides some information of the complex vortex motion associated with vortexline reconnection.

Consider a problem that the initial state is given in such a way that two vortex rings are set to move along the paths intersecting at right angles at the origin and collide with one another. The bisecting straight line between the two paths of the vortex center is taken as the polar axis $\theta = 0$ (along the x_3 axis) of the spherical coordinate system. The plane perpendicular to the x_3 axis is the (x_1, x_2) plane on which $\theta = \pi/2$. There are two symmetry planes including the x_3 axis: one includes the trajectories of the vortex centers which is defined as (x_2, x_3) plane and the plane (x_1, x_3) perpendicular to it is also a symmetry plane which bisects the two trajectories. The plane $\phi = 0$ is taken along the positive x_1 axis. From the geometrical arrangement just mentioned, the acoustic pressure $p(\theta, \phi, t)$ is characterized by the symmetry:

$$p(\theta, -\phi, t) = p(\theta, \phi, t), \quad p(\theta, \phi + \pi, t) = p(\theta, \phi, t). \quad (8)$$

The formula (2) is rewritten by using the spherical polar coordinates (r, θ, ϕ) : $x_1 = r \sin \theta \cos \phi$, $x_2 = r \sin \theta \sin \phi$, $x_3 = r \cos \theta$. In view of the symmetry (8), the pressure is represented as

$$\begin{aligned} p(\theta, \phi, t) = & A_0(t) + A_1(t)P_2^0(\cos \theta) + A_2(t)P_2^2(\cos \theta) \cos 2\phi \\ & + B_1(t)P_3^0(\cos \theta) + B_2(t)P_3^2(\cos \theta) \cos 2\phi, \end{aligned} \quad (9)$$

where higher order terms are omitted since observed amplitudes are not significant. Thus it is found that the far-field acoustic pressure (2) is represented in terms of the

five normal modes with five coefficient functions of time $[A_0(t), A_1(t), A_2(t), B_1(t), B_2(t)]$. Here the Legendre functions are $P_2^0 = (1/2)(3\cos^2\theta - 1)$, $P_2^2 = 3\sin^2\theta$, ..., and $P_3^0 = (1/2)(5\cos^3\theta - 3\cos\theta)$, $P_3^2 = 15(\cos\theta - \cos^3\theta)$,

Observation: The acoustic waves emitted by the 90° collision were detected at 102 different angular positions on the three great circles of radius $r = 620\text{mm}$ on the three orthogonal planes: (1) $\phi = \pi/2, 3\pi/2$; (2) $\phi = 0, \pi$; (3) $\theta = \pi/2$. The trajectories of the vortex cores in the (x_2, x_3) plane observed by a photosensor are shown in Figure 4, where the ring radius $R_0 = R(0)$ of the single (unperturbed) vortex was 4.7mm.

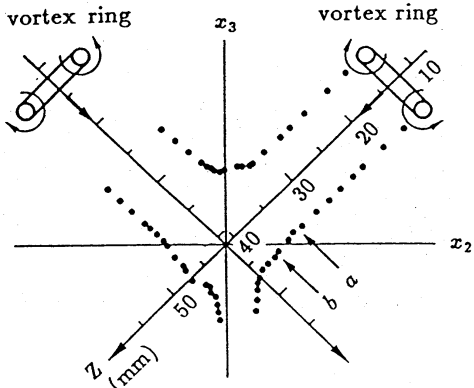


Figure 4. Observed core trajectories of two colliding vortices in the (x_2, x_3) plane including the vortex center. The marked positions a and b correspond to the times of Figure 5 (broken lines).

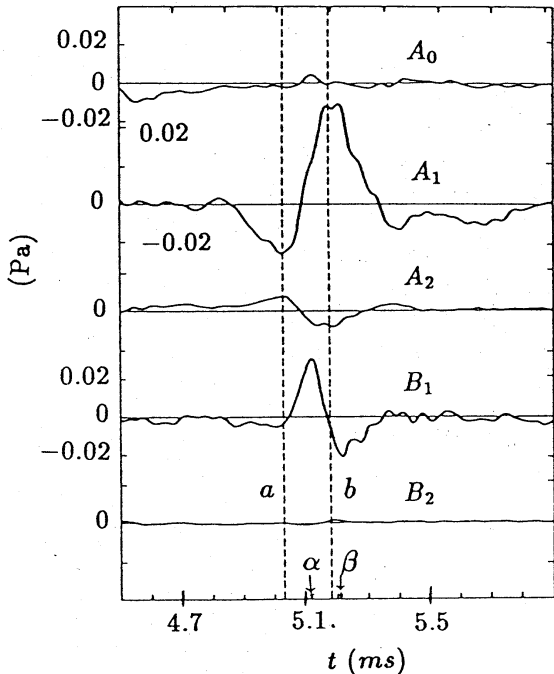


Figure 5. Main mode amplitudes of observed waves.

The symmetry relation (8) is found to be consistent with the observed data. In fact, the acoustic pressure detected in the plane $\theta = \pi/2$ can be expanded into Fourier series with respect to the angle ϕ , and it is found that the Fourier coefficients of $\sin m\phi$ ($m = 1 \sim 4$) and $\cos m'\phi$ ($m' = 1, 3, 4, 5$) are negligible. Three sets of profile functions of $[A_0, A_1, A_2, B_1, B_2]$ can be determined from the observed data. It is found that they coincide almost with each other. These profiles are shown in Figure 5.

Computation: A computer simulation [15] of the vortex collision is newly carried out in order to have more realistic estimation of the acoustic emission than the previous one [7], using the method of *vorticity and vector potential* [16]. The viscous incompressible vorticity equation is solved numerically, together with the continuity equation, by a new algorism on 141^3 grid points. Boundary condition of zero-vorticity is imposed on the cubic bounding surface.

The isotropic component is proportional to the second time derivative of the kinetic energy from (2) and (6), and the quadrupole components and higher modes are related to the change of moments of vorticity distribution. Using the data from the simulation, we can calculate the tensors $Q_{ij}(t)$ and $Q_{ijk}(t)$ of (4) and (5). Thus we readily obtain the main mode coefficients $[\tilde{A}_0, \tilde{A}_1, \tilde{A}_2, \tilde{B}_1, \tilde{B}_2]$. It is remarkable that the main mode amplitudes obtained from the computation are in quantitative agreement with the observed ones, unlike the previous computation for fatter cores of vortex.

Significance of dominant wave modes: Observed amplitudes A_1 and A_2 of the two quadrupoles P_2^0 and $P_2^2 \cos 2\phi$ in (9) are significantly large. There exists non-negligible amplitude in the monopole. Out of the two third-order components, the amplitude B_2 of $P_3^2 \cos 2\phi$ is negligibly small, while significant amplitude of the mode P_3^0 is observed. To see the significance of the wave signals, let us look into the distributions of the wave source. The amplitudes $A_1(t)$ and $B_1(t)$ are represented by the integrals,

$$A_1(t) = \int a_1(\mathbf{y}, t) d^3 y, \quad a_1(\mathbf{y}, t) = -\frac{1}{12\pi} y_3 p_3^{(3)}(\mathbf{y}, t)$$

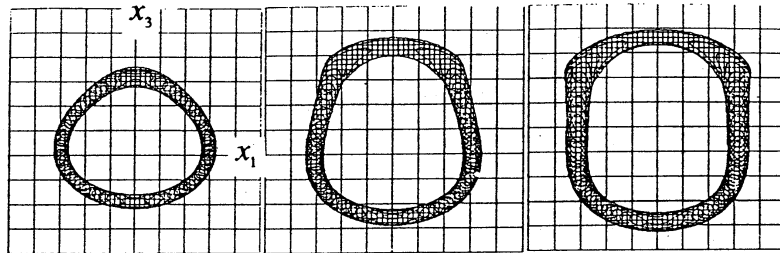
$$B_1(t) = \int b_1(\mathbf{y}, t) d^3 y, \quad b_1(\mathbf{y}, t) = \frac{1}{32\pi} (y_3^2 - \frac{1}{5} y^2) p_3^{(4)}(\mathbf{y}, t)$$

where

$$p_3 = (\mathbf{y} \times \boldsymbol{\omega})_3.$$

The integrands $a_1(\mathbf{y}, t)$ and $b_1(\mathbf{y}, t)$ are considered to represent the source distributions of each wave mode. In figure 6, distribution of the source function $b_1(\mathbf{y}, t)$ is projected to the plane (x_1, x_3) (viewed from the x_2 axis) at three times: the time α (positive B_1 peak), the time b (positive A_1 peak) and the time β (negative B_1 peak), where projected contours of the iso-vorticity surface are also plotted at the corresponding times. It is remarkable that the wave sources at the times b and β are localized in the upper left and right regions where reconnection of vortex lines are observed. This is considered to be a first identification of the acoustic signal related to the vortex-line reconnection.

(a) Iso-vorticity contour



(b) Source function $b_1(t)$

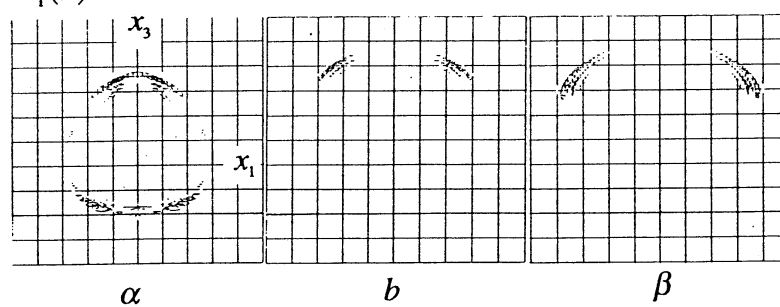


Figure 6. Projection diagrams in the plane (x_1, x_3) of (a) the iso-vorticity surfaces and (b) the source function $b_1(\mathbf{y}, t)$ at the three times: α , b and β (see Fig. 5).

5. Interaction of a Vortex Ring with a Shock Wave

Problems of strong interaction between a rotational motion and compressive waves are suited for computational study. Recently, experimental investigation is made for an axisymmetric problem of strong shock-vortex interaction [17], and computer simulations show significant nonlinear effects in the interaction of a shock wave with a vortex. This section is a brief account of a computational study by Takayama *et al.* [18] to simulate the experiment.

The computer simulation is carried out by discretizing the axisymmetric forms of the conservation laws of mass, momentum and energy for a viscous and heat-conducting gas model supplemented by the species conservation equation. Time integration of the hyperbolic set of partial differential equations is made by the explicit second-order MacCormac method, complemented by the shock capturing FCT smoothing technique [19]. Initially a vortex ring is generated in the computational domain by driving a shock wave of nitrogen gas (with Mach number 1.4) through a small circular orifice into a cylindrical tube of much larger dimension (Figure 7). Another plane shock wave (driven at the other end of the tube) is advancing from the opposite direction, which is shot at a later time and impinging on the vortex with a *shock disk*, after interacting with the first wave. The gaseous fluid in the cylindrical tube is assumed to consist of nitrogen and oxygen, being at rest initially, with the pressure p_0 , temperature T_0 and specific heat ratio γ set as $p_0 = 101.3 \text{ kPa}$, $T_0 = 300 \text{ K}$ and $\gamma = 1.3982$, respectively. The normalization parameters are given such that $l_0 = 1 \text{ cm}$ and $t_0 = 1 \mu\text{sec}$. The results are obtained for the mesh size of $\Delta x/l_0 = \Delta r/l_0 = 0.01$ and the starting time of the second shock wave was at $t_2/t_0 = 108$ from the first shock.

A remarkable property found in the simulation is that, during the passage of the shock wave over the vortex ring, the part of the wave propagating through the inside of the ring-vortex is intensified spontaneously at a localized region (Figure 8). Maximum pressure occurs inside the vortex and attains a high value, about several times that of the impinging shock of Mach number of around 1.2, the vortex translation Mach number being 0.60 (Figure 9).

From detailed study of the structure of the interaction, it is found that there exists a gas dynamic mechanism of intensification of shock waves in the flow field in which two step processes are observed. The double-step mechanism of the self-intensification consists of the first slight intensification of the impinging shock wave by the interaction with the opposing flow due to the vortex, and the second intensification by the convergence of outer diffracted shock wave around the vortex on the central axis at the back of the vortex ring. A possible application of the present mechanism is the spontaneous ignition of a gas mixture with a reactive component by a shock wave.

Acknowledgement: The author wishes to gratefully thank Dr. S. Adachi and Prof. K. Ishii and also Profs. T. Minota and F. Takayama for collaborative work on various aspects of the present subjects.

REFERENCES

- 1 A. Powell, *J. acoust. Soc. Am.*, **36** (1964) 177.
- 2 S.C. Crow, *Stud. appl. Math.*, **49** (1970) 21.
- 3 W. Möhring, *J. Fluid Mech.* **85** (1978) 685.
- 4 T. Kambe and T. Minota, *Proc. R. Soc. Lond.*, **A386** (1983) 277.
- 5 T. Kambe, *J. Fluid Mech.* **173** (1986) 643.
- 6 E.-A. Müller and F. Obermeier, *Fluid Dyn. Res.* **3** (1988) 43.
- 7 T. Kambe, T. Minota and M. Takaoka, *Phys. Rev. E* **48** (1993), 1866.
- 8 M.J. Lighthill, *Proc. R. Soc. Lond.*, **A211** (1952) 564.
- 9 T. Kambe and T. Minota, *J. Sound Vib.* **74** (1981) 61.
- 10 T. Kambe, in *Theoretical and Applied Mechanics 1992* (eds: S.R. Bodner, J. Singer & A. Solan; Elsevier), 239-255 (1993).
- 11 T. Kambe, *J. Sound Vib.* **95** (1984) 351.
- 12 K. Shariff, A. Leonard and J.H. Ferziger, NASA Tech. Mem. 102257 (1989).
- 13 T. Kambe and U Mya Oo, *J. Phys. Soc. Jpn.* **53** (1984) 2263.
- 14 T. Minota and T. Kambe, *J. Sound Vib.* **111** (1986) 51.
- 15 K. Ishii, S. Adachi and T. Kambe, "Acoustic signals associated with vortexline reconnection in oblique collision of two vortex rings", in preparation (1995).

- 16 K. Ishii, K. Kuwahara and C.H. Liu, *Computers & Fluids* **22** (1993), 589.
 17 T. Minota, *Fluid Dyn. Res.* **12** (1993), 335.
 18 F. Takayama, Y. Ishii, A. Sakurai & T. Kambe, *Fluid Dyn. Res.* **12** (1993), 343.
 19 T. Kambe and F. Takayama, "Compressive vortex ring and interaction with shock waves" in *Computational Fluid Dynamics* (Proc. of Les Houches Summer School 1993; Elsevier), to appear in 1995.

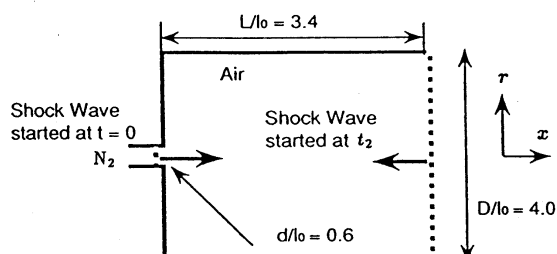


Figure 7. Computational domain and setup.

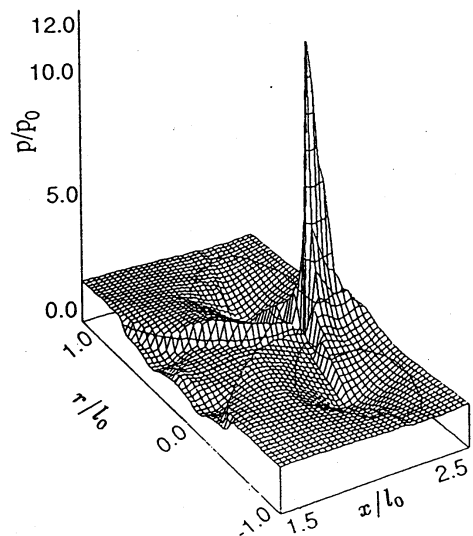


Figure 9. Perspective pressure plot
at $t/t_2 = 153.32$.

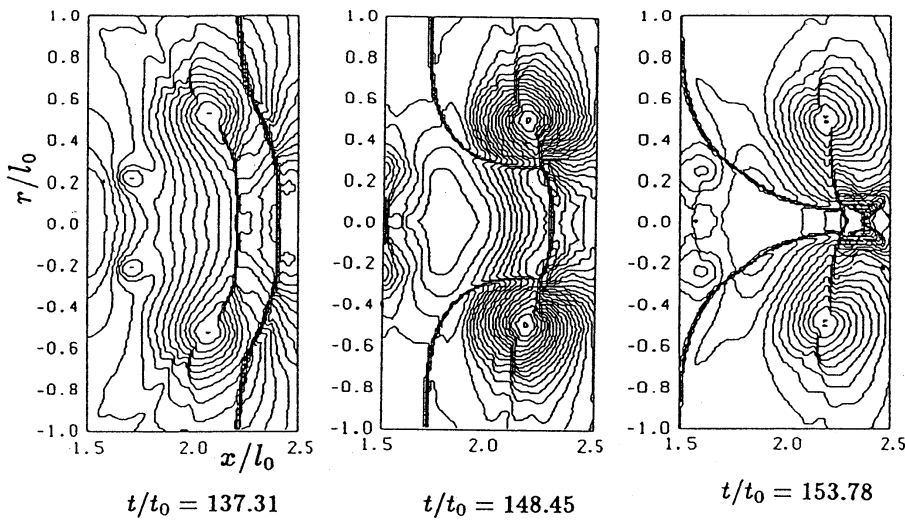


Figure 8. Pressure contours at three times for $M_2 = 1.225$.